AIAA Aviation
22-26 June 2015, Dallas, TX
AIAA Atmospheric Flight Mechanics Conference

Minimum Terminal Energy Optimizations of Hypersonic Vehicles Using Indirect Methods

Michael J. Grant*
Purdue University, West Lafayette, IN, 47906
Michael A. Bolender†
Air Force Research Laboratory, Wright-Patterson Air Force Base, OH, 45433

In this investigation, relevant aerospace problems of interest that involve solutions with minimum terminal energies are solved using indirect methods. The required considerations to solve this class of problems is discussed, and the solutions verify that the phugoiding trajectories of high energy systems satisfy the necessary conditions of optimality. An example footprint analysis and boost-glide reconnaissance application demonstrate the quality of solutions obtained using the indirect methodology. Comparisons with a modern trajectory optimization tool, DIDO, validate the indirect optimization framework used to construct solutions in this investigation.

Nomenclature

ang	replacement control	T	thrust
D	drag force magnitude	t	time
L	lift force magnitude	v	relative velocity
m	mass	nd	nondimensional
r	radial magnitude		
α	angle of attack	ϕ	latitude
γ	relative flight-path angle	ψ	relative heading
μ	gravitational parameter	σ	bank angle
ω	rotation rate of planet	θ	longitude

I. Introduction

Traditionally, the mission design of hypersonic systems is accomplished by solving the optimal control problem under a specific set of simplifying assumptions[1–3] or by using direct optimization methods.[4–7] In Ref. 1, a rapid footprint methodology is presented that solves the optimal control problem for quasi-equilibrium glide flight. In the investigation, the maximum crossrange problem associated with footprint generation is converted to a closest-approach problem of virtual targets. This conversion in problem formulation is performed by noting that convergence could not be obtained otherwise. The trajectory optimization problem was further simplified by fixing the angle of attack profile (common for equilibrium glide applications), requiring only optimal bank angle solutions. In Refs. 2 and 3, an elaborate derivation of the necessary conditions of optimality is performed for a hypersonic cruise vehicle in which solutions are obtained for constant altitude flight with either a constant velocity or a prescribed deceleration profile. This simplified problem was used to validate the optimal solutions obtained by GPOCS. For the three dimensional trajectory

*Assistant Professor, School of Aeronautics and Astronautics, AIAA Senior Member.
†Senior Aerospace Engineer, AIAA Associate Fellow.

optimization also performed, the covectors obtained from GPOCS were used to determine the optimal control profiles derived from the necessary conditions of optimality. Comparisons to the GPOCS optimal control history provided confidence in the quality of the GPOCS solution. In Ref. 4, a real-time footprint algorithm is proposed for near equilibrium glide entries. A collocation method within ASTOS is used to identify significant features of the designed angle of attack profile. It is also noted that for near equilibrium glide entries, the vehicle spends a significant amount of time flying at peak L/D in order to maximize the distance flown. To assist with the real-time generation of footprints, reference-based controllers in altitude and flight path angle were used.

In Ref. 5, it is noted that the complexities associated with solving the necessary conditions as a two-point boundary value problem prevents the approach from being a viable option to generate generic footprints. To bypass these complexities without resorting to simplifying assumptions of the equations of motion, a Legendre pseudospectral method contained within the DIDO software package is used to generate footprints. Comparisons are made to optimal control solutions of a reduced order model to highlight the improved solutions obtained from DIDO. In Ref. 6, a Gauss pseudospectral method is used to generate various optimal hypersonic trajectories using the GPOPS software package. Comparisons to POST were made to highlight the improved solutions obtained using the GPOPS software. In Ref. 7, a DIDO solution to an entry problem was compared to a subset of the necessary conditions of optimality. The covectors obtained from DIDO were used to calculate the optimal controls obtained from the necessary conditions of optimality. Comparisons to the DIDO control history provided confidence in the DIDO solution. Additionally, the Hamiltonian was verified to be a near constant value of zero as required by the necessary conditions of optimality.

In all cases, the use of direct optimization methods is preferred over optimal control theory to generate complex non-simplified optimal trajectories of interest. As such, these methods serve a practical means of performing complex trajectory optimization in which portions of the necessary conditions of optimality from optimal control theory are used as a checking mechanism to verify the quality of the direct solution. The common checks that are performed consist of using the covectors to create the corresponding control and Hamiltonian values associated with optimal control theory. Comparisons to the direct control history and the expected constant Hamiltonian value of zero (for typical trajectory optimization problems) provide confidence in the quality of the direct solution. This overall solution approach is particularly appealing because it overcomes the three historical limitations that arise when solving the full optimal control problem:[8]

1. Approach requires knowledge of optimal control theory and the development of lengthy necessary conditions of optimality.

2. If the problem contains path inequalities, it is necessary to make an *a priori* estimate of the constraint-arc sequence.

3. It is difficult to provide a good initial guess, especially in costates, to converge to a solution.

Prior research by Grant has demonstrated that the historical optimal control challenges associated with indirect optimization methods can be largely overcome to perform hypersonic mission design. The creation of the necessary conditions of optimality is performed in a completely automated fashion by leveraging modern symbolic computational tools such a Mathematica. By formulating the optimality conditions in a generic fashion, the application of appropriate boundary conditions associated with various constraint arc sequences can be dynamically enforced by employing a continuation process.[9,10] Additionally, by solving a sequence of progressively difficult optimization problems via continuation, it is possible to create complex optimal trajectory solutions that fully satisfy the necessary conditions of optimality without supplying a good initial guess to the complex solution.

As an example, an indirect solution can be easily constructed for a short, unconstrained, minimum heat load trajectory as shown in Fig. 1. While this trajectory is of little interest to the designer, the optimal solution can be easily and rapidly evolved to the desired optimal solution using indirect optimization methods. This is accomplished by first extending the trajectory to match the desired initial and terminal conditions as shown in Fig. 2. After this process is completed, heat rate and g-loading constraints can be introduced and incrementally reduced to the desired value as shown in Figs. 3 and 4. As a result, complex trajectory solutions can be rapidly constructed through a sequence of progressively difficult optimization problems. In this framework, the derivation of the necessary conditions of optimality, application of appropriate multi-point boundary conditions throughout the continuation process, and management of the continuation parameters is performed in an automated manner that is transparent to the designer. This automation has greatly reduced

the historical burden of using optimal control theory to perform rapid mission design. In this example and in the examples provided in this investigation, Mathematica is used to develop the necessary conditions of optimality, and Matlab scripts are automatically generated with this information. The scripts are then automatically autocoded to C, and the resulting boundary value problems are solved using Matlab's *bvp4c*. As such, the challenge of using optimal control theory is reduced to selecting an appropriate continuation process.

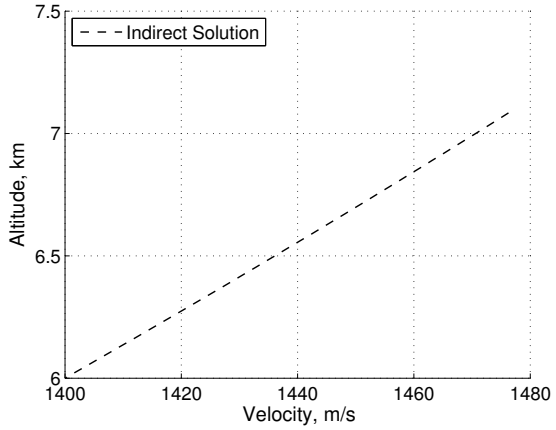

Figure 1: Initial indirect solution.

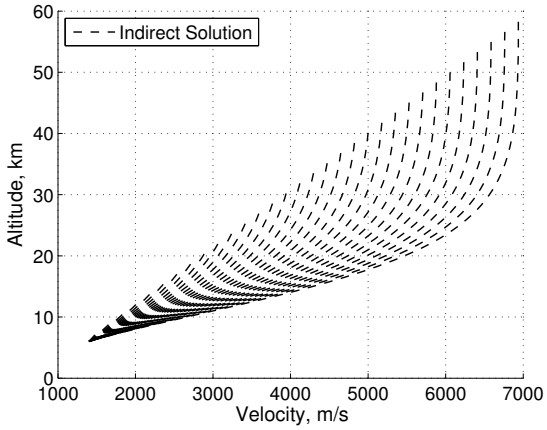

Figure 2: Trajectories from unconstrained continuation.

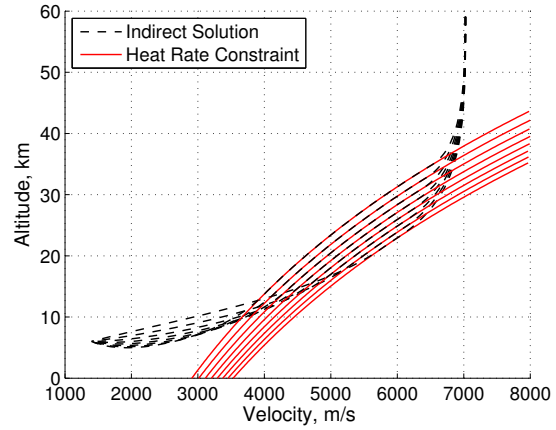

Figure 3: Trajectories from continuation of heat rate constraint.

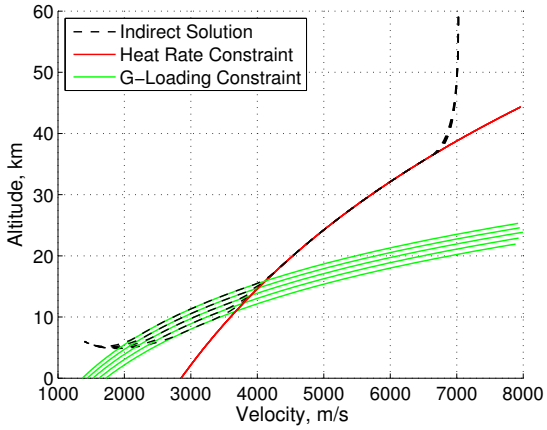

Figure 4: Trajectories from continuation of g-loading constraint.

In this investigation, two trajectory optimization examples that consist of minimum terminal energy states are provided to illustrate the manner in which solutions are generated using the optimal control framework. In the first example, a footprint of maximum size is constructed without resorting to trajectory simplifications. Comparisons with DIDO solutions illustrate the quality of solutions obtained using the optimal control framework. In the second example, a maximum range, boost-glide reconnaissance trajectory is also generated without trajectory simplifications. While the optimal control framework can also automatically incorporate path constraints (as shown in Figs. 3 and 4), consideration was given to challenging trajectories without path constraints. The framework enhancements from the initial research described in Refs. 9 and 10 required to solve these types of challenging trajectory problems is described below.

II. Extension of The Optimal Control Framework to Support Minimum Terminal Energy Studies

The prior example illustrates the ability to solve the optimal control problem for a planar hypersonic entry with a single control (bank angle) and simplified aerodynamics (drag polar) and atmosphere (exponential) models. In this investigation, the optimal control framework is extended to incorporate higher fidelity models that are typically used with modern trajectory optimization tools. The following enhancements enable the rapid construction of vehicle capability boundaries by solving the full optimal control problem.

II.A. Extension to Full 3DOF Motion with Scaling

The optimal control framework was extended to include an arbitrary number of degrees of freedom and number of controls. This enabled the creation of optimal control solutions without simplification of the equations of motion (shown in Eqs. (1)-(6)) or imposing any other assumptions about the flight profile. During the continuation process, the states, costates, and all other parameters of the optimization problem are nondimensionalized to enable convergence to the complex solutions. Since the nondimensionalization is often connected to the maximum values of states, each problem solved during the continuation process is re-nondimensionalized in an automated manner using information from the previous optimal solution. This process eliminates the need for the designer to properly scale complex problems.

$$\frac{dr}{dt} = v\sin\gamma \tag{1}$$

$$\frac{d\theta}{dt} = \frac{v\cos\gamma\cos\psi}{r\cos\phi} \tag{2}$$

$$\frac{d\phi}{dt} = \frac{v\cos\gamma\sin\psi}{r} \tag{3}$$

$$\frac{dv}{dt} = \frac{T-D}{m} - \frac{\mu\sin\gamma}{r^2} + \omega^2 r\cos\phi(\sin\gamma\cos\phi - \cos\gamma\sin\phi\sin\psi) \tag{4}$$

$$\frac{d\gamma}{dt} = \frac{L\cos\sigma}{mv} - \frac{\mu\cos\gamma}{vr^2} + \frac{v\cos\gamma}{r} + 2\omega\cos\phi\cos\psi + \omega^2 r\cos\phi(\cos\gamma\cos\phi + \sin\gamma\sin\phi\sin\psi) \tag{5}$$

$$\frac{d\psi}{dt} = \frac{L\sin\sigma}{mv\cos\gamma} - \frac{v\cos\gamma\cos\psi\tan\phi}{r} + 2\omega(\tan\gamma\cos\phi\sin\psi - \sin\phi) - \frac{\omega^2 r\sin\phi\cos\phi\cos\psi}{v\cos\gamma} \tag{6}$$

II.B. Automated Control Selection

During formulation of the necessary conditions of optimality, it is possible to identify multiple candidate control solutions. While solving the boundary value problem, all candidate control solutions are evaluated each time a control value must be calculated. The appropriate candidate control is selected based on Pontryagin's Minimum Principle which provides additional confidence in the optimality of the numerical solutions.

II.C. Incorporation of High Fidelity Routines

The simple planar example in Section I consisted of simple aerodynamic and atmospheric models. To support more relevant studies of vehicle capability, the optimal control framework has been extended to also enable trajectory solutions using high fidelity aerodynamic information (*e.g.*, from computational fluid dynamics) and high fidelity atmospheric information (*e.g.*, from Earth GRAM or standard atmosphere profiles). Since the necessary conditions of optimality are formulated symbolically, an assessment is made as to whether or not each individual necessary condition can be formulated analytically. If an analytic formulation is not possible, then the necessary conditions are formulated numerically in which derivatives are computed using the complex step method.

II.D. Incorporation of Smoothed Bang-Bang Control and Singular Arcs

To support thrusting applications in this investigation, a smoothing algorithm described in Ref. 11 has been incorporated into the optimal control framework. This smoothing approach introduces artificial controls into each equation of motion that does not contain any physical control variables. During the solution process, the artificial control variables are scaled to near-zero values, thereby ensuring that the solution to the smoothed problem converges to the solution of the original problem. The smoothing enables continuous derivatives to be calculated across the bang-bang control structure and also enables convergence to trajectories that contain singular arcs. The optimal control framework is capable of automatically identifying bang-bang control structures within the necessary conditions of optimality, and the framework automatically incorporates the artificial controls necessary to provide smoothing of the bang-bang control structure.

With these advancements, a largely automated process has been developed that only requires user input of the optimization problem, algorithm settings, and continuation policy. As such, nearly all of the functionality is performed transparently to the designer. While current efforts are focused on the automated selection of the continuation policy, the policies in this investigation were chosen from experimentation. In the following examples, hypersonic trajectories are optimized with various combinations of control in angle of attack, α, bank angle, σ, and thrust, T.

III. Minimum Energy Terminal State Optimizations Using Indirect Methods

Many hypersonic problems of interest consist of the determination of vehicle performance limitations in downrange and/or crossrange. These applications generally result in a situation where the vehicle flies to a minimum terminal energy state. The optimal control formulation provides great insight into the optimal behavior of such systems, and particular considerations must be made in order to overcome the historical challenges described in Section I.

III.A. Optimal Angle of Attack Control Law

Since the necessary conditions of optimality are formulated symbolically using Mathematica, it is often intractable to directly analyze the resulting expressions that frequently span many thousands of characters. For complex, high order aerodynamic models that are function of angle of attack and Mach number, the optimal angle of attack control law is of similar complexity. However, the fundamental optimal behavior of vehicles modeled in this manner can be understood by analyzing a vehicle that exhibits a traditional drag polar with aerodynamics described by Eqs. (7) and (8).

$$C_L = C_{L,0} + C_{L,\alpha}\alpha \tag{7}$$

$$C_D = C_{D,0} + C_{D,\alpha}\alpha + C_{D,\alpha^2}\alpha^2 \tag{8}$$

Since optimal vehicle performance trajectories are generally only a function of the terminal state (*e.g.*, to maximize downrange and/or crossrange, etc), the optimal angle of attack control law is independent of the objective functional. For portions of the trajectory with a zero bank angle (common during the terminal portion of optimal vehicle performance trajectories), the optimal angle of attack control law for a vehicle with a traditional drag polar is shown in Eq. (9).

$$\alpha = \frac{1}{2C_{D,\alpha^2}}\left(\frac{\lambda_\gamma}{v\lambda_v}C_{L,\alpha} - C_{D,\alpha}\right) \tag{9}$$

It is common in vehicle performance studies to have a free terminal velocity that does not appear in the cost functional. For these cases, the necessary conditions of optimality dictate that λ_v must be zero at the terminal point, resulting in a singularity in the calculation of angle of attack as described by Eq. (9). This singularity is consistent with the fact that the vehicle would want to produce greater lift as the terminal point is approached in order to maximize the glide range of the vehicle. To easily bound the angle of attack and avoid the singularity at the terminal point, a smooth function shown in Eq. (10) is used, where a_1 and a_2 are chosen based on the desired limits in angle of attack. In this approach, the angle of attack becomes an intermediate variable and the variable *ang* becomes the replacement control. This formulation enables convergence to maximum vehicle performance optimal control solutions. The following maximum footprint

and long range reconnaissance examples demonstrate the quality of solutions obtained using this approach in which the necessary conditions of optimality are satisfied at all locations along each trajectory. To prevent the release of sensitive information, all of the results presented in this investigation are nondimensionalized.

$$\alpha = a_1 \sin(\text{ang}) + a_2 \tag{10}$$

III.B. Maximum Footprint Generation

In this example, a high quality footprint is created for a high L/D hypersonic vehicle in which no simplifying assumptions are made to the original equations of motion. Additionally, both the angle of attack (through the surrogate control, *ang*) and bank angle profiles are optimized to characterize the worst case distances that could be travelled due to a loss of control. The atmosphere is modeled using the Standard 1976 Atmosphere, and the vehicle aerodynamics is modeled from high fidelity information derived from computational fluid dynamics. In this analysis, crossrange is maximized at fixed downrange increments, resulting in the minimizing functional shown in Eq. (11), where the terminal latitude, ϕ_f, is maximized to construct the upper portion of the footprint. The initial state of the vehicle is fully specified according to anticipated due-West post-boost staging conditions such that downrange is oriented along a constant latitude.

$$J = -\phi_f \tag{11}$$

III.B.1. Continuation Procedure

The optimal control framework overcomes many of the historical limitations associated with converging to complex optimal control solutions. The remaining challenge requires the designer to identify the appropriate continuation sequence to arrive to the complex solutions in a manner analogous to the planar example described in Section I. This is accomplished by noting that it is generally easier to initially construct short optimal trajectories and sequentially evolve to the long trajectories associated with the footprint analysis. The continuation procedure is initiated by reverse integrating a one second trajectory from a terminal point at the ground. Noting that the latitude is maximized along the upper portion of the footprint, the terminal heading is selected as 90 deg (due North). A guess of zero is chosen for all terminal costates except for the costate associated with latitude which was chosen according to Eq. (12). The states resulting from the reverse integration are constrained at the initial point of the trajectory, and the terminal altitude and longitude are constrained. Convergence to the indirect solution using this initial guess is relatively easy. Starting with this initial optimal solution, the initial state of the vehicle is incrementally (but rapidly) modified to match the anticipated post-boost staging conditions using two continuation phases. During the first continuation phase, the initial velocity is partially increased and altitude fully increased to the desired initial values as shown in Fig. 5. Additionally, the initial heading and terminal longitude are modified to a westerly direction as shown in Fig. 6. During the second continuation phase, the initial velocity (shown in Fig. 7) and flight-path angle are modified to the desired initial values. At the end of this process, a solution is created that exists on the footprint as shown in Fig. 8.

$$\lambda_{\phi,f} = -1 \tag{12}$$

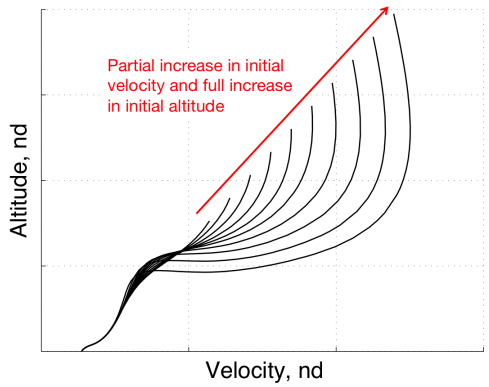

Figure 5: Energy history associated with first continuation phase.

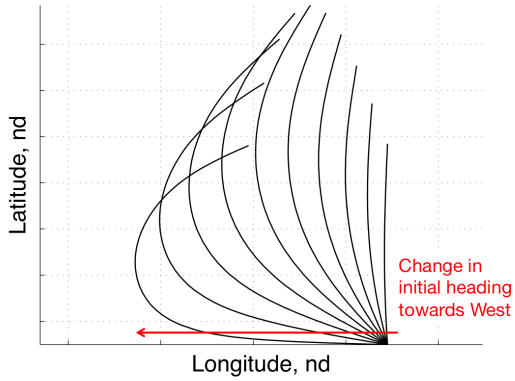

Figure 6: Evolution of maximum crossrange trajectory during first continuation phase.

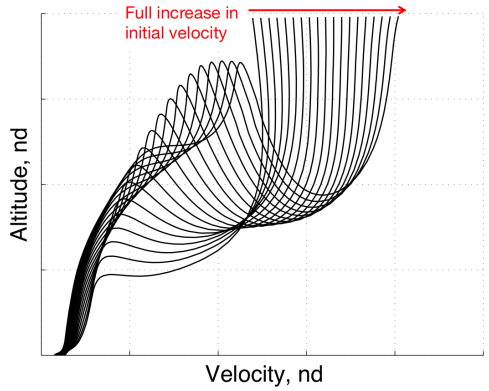

Figure 7: Energy history associated with second continuation phase.

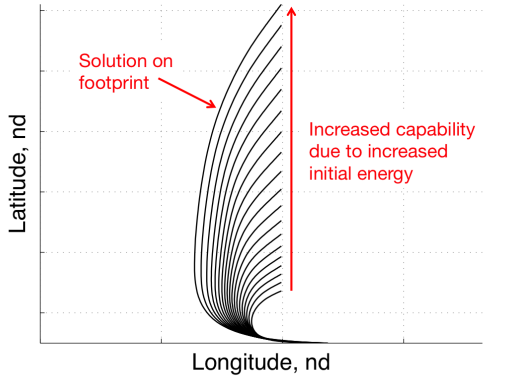

Figure 8: Evolution of maximum crossrange trajectory during second continuation phase.

III.B.2. Footprint Comparison

After the aforementioned process is completed, a continuation in terminal downrange is performed to construct the upper portion footprint as shown in Fig. 9. This process is repeated for the minimizing cost functional shown in Eq. (13) to construct the lower portion of the footprint. For validation, the corresponding DIDO solutions are also shown in Fig. 9. As shown, the overall footprint size and shape are consistent between the two approaches. Due to the shallow initial flight path angle, exclusion zones exist at the heel of the footprint. Note that the necessary conditions of optimality are fully satisfied along each indirect trajectory of the footprint. The aggressive turns associated with the footprint generation illustrate that that complex trajectories with realistic atmospheric and aerodynamic models can be constructed in a nearly automated manner using optimal control theory. However, the selection

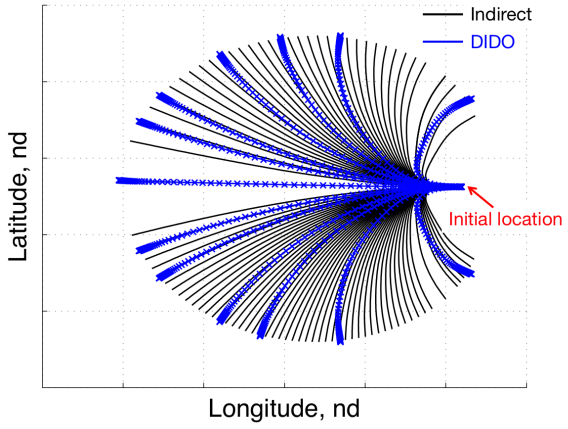

Figure 9: Footprint of a high L/D hypersonic vehicle.

of the continuation policy as described above is not a trivial task to accomplish.

$$J = \phi_f \tag{13}$$

Due to the overall symmetry of the footprint, the following trajectory comparisons consist of only trajectories that reside in the upper portion of the footprint. Figs. 10 and 11 illustrate the energy and flight-path angle histories associated with the various footprint trajectories. While numerous indirect solutions are used to highlight the overall range in trajectory parameters across the upper footprint solutions, note that the overall trend of each indirect solution closely resembles the DIDO solutions presented. Trajectories associated with large downranges remain shallow by phugoiding at high altitudes. Alternatively, trajectories that require aggressive turns (e.g., to terminate at longitudes behind the initial location of the vehicle) perform an aggressive dive. While this dive increases the drag of the vehicle, it enables an early turn to capture the heel of the footprint. The aggressive dive is followed by an aggressive loft (as noted by the rapid shift in flight-path angle during the early portion of the trajectory) to increase timeline and, therefore, crossrange. A similar behavior is observed from the DIDO solutions. Note that all of the indirect trajectories terminate at precisely the same flight-path angle. This is expected as the vehicle performs a maximum lift glide at the relatively slow terminal velocities. Note that the minor terminal flight-path angle artifacts observed by the DIDO solutions do not substantially alter the performance of the trajectory. Also note that the terminal flight-path angles from DIDO nearly match the optimal indirect solutions. These comparisons further validate that the optimal control framework is functioning as expected.

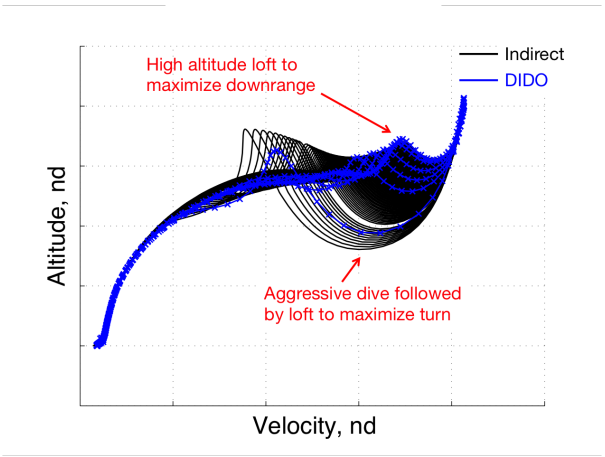

Figure 10: Energy history associated with upper footprint.

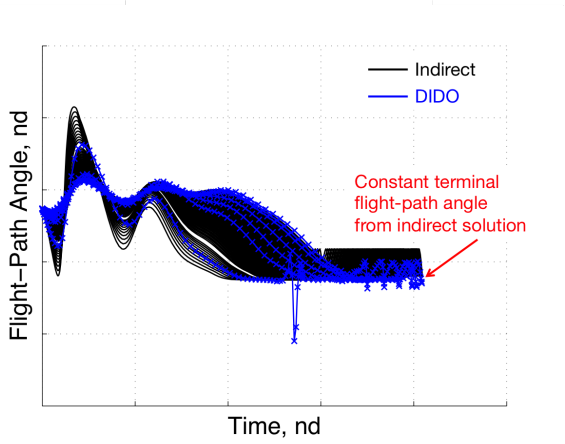

Figure 11: Flight-path angle vs. time associated with upper footprint.

The complex control histories shown in Fig. 12 highlight the quality of solutions that are made possible by the use of the optimal control framework. The necessary conditions of optimality are fully satisfied along every point of each footprint trajectory. As such, the complex early maximum lift maneuvers used to initiate a high altitude phugoid trajectory as well as late maximum lift maneuvers to perform aggressive turns are captured with high quality. Since these high quality solutions leverage optimal control theory, the explicit optimal relationship between angle of attack and bank angle control (expressed as a function of the states and costates) is leveraged along each optimal solution. Note that the DIDO solutions do not exhibit the mid-trajectory, high lift maneuvers. Instead, the DIDO solutions exhibit commanded angles of attack that are beyond the constrained upper limit represented by the flat indirect angle of attack regions. Other than the observed numerical artifacts at the terminal portion of the trajectory, the indirect and DIDO bank angle profiles exhibit a similar structure.

Due to the lack of agreement in the angle of attack control profiles between DIDO and the indirect solutions, it is expected that the costates would also not agree. As such, no meaningful comparison can be performed. The costates associated with the optimal control problem are shown in Fig. 13. As expected, the costates satisfy the necessary conditions of optimality. Since the terminal flight-path angle, terminal heading, and terminal velocity are free, the corresponding costates terminate at zero. Additionally, the terminal latitude costate terminates at negative one as expected for solutions along the upper portion of the footprint. Since the costates are well behaved, convergence to the indirect solutions is not problematic.

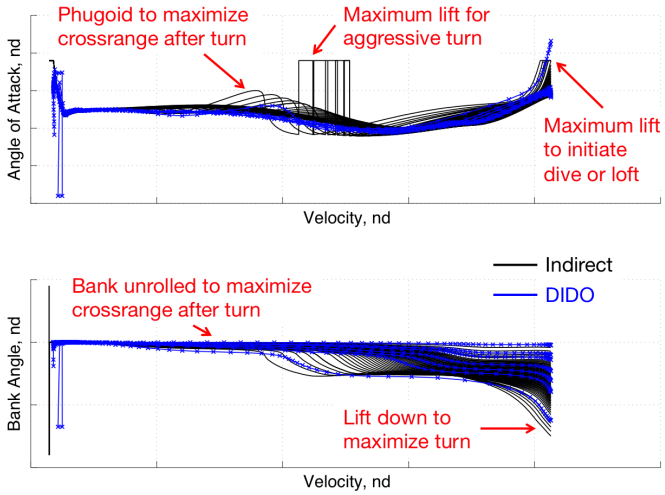

Figure 12: Optimal control histories associated with upper footprint.

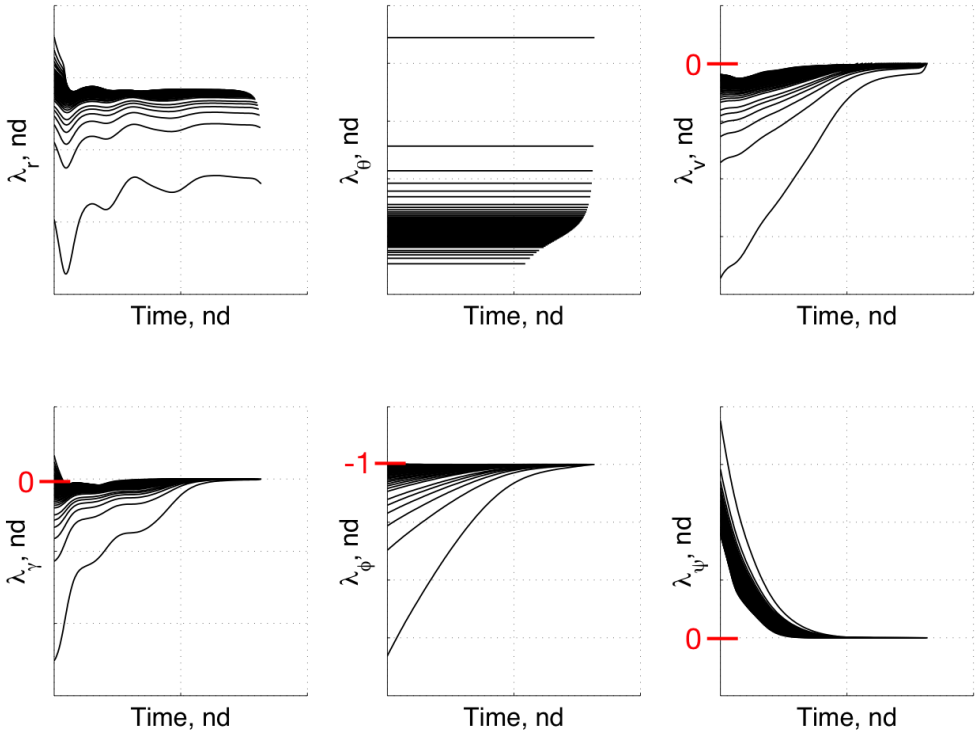

Figure 13: Costate histories associated with upper footprint.

III.C. Boost-Glide Reconnaissance Application

While the prior footprint example demonstrates a capability to perform higher fidelity, indirect trajectory optimization to construct high quality trajectories, the vehicle is assumed to be unpowered. The ability to incorporate powered flight within the optimal control framework is particularly challenging due to the possibility of control switches and singular arcs.[12] To support long range boost-glide reconnaissance applications, an automated control smoothing algorithm was incorporated that is able to account for these control considerations while also providing continuous derivative information during the numerical root solving process associated with the two point boundary value problem.[11] In the following example, a hypersonic reconnaissance system is boosted to a high altitude after being released from a carrier aircraft, and angle of attack and thrust profiles are optimized to maximize downrange (as described by Eq. (14)), allowing the vehicle to be deployed and recovered in friendly territory. In this example, vehicle aerodynamics are also derived from computational fluid dynamics, and the Standard 1976 Atmosphere is used. Additionally, planar motion was only considered for this analysis in which downrange was measured along longitude.

$$J = -\theta_f^2 \tag{14}$$

To solve this problem, the vehicle mass is added as a state, and a continuation process is employed that varies terminal mass as shown in Fig. 14. Initially, the mass of the vehicle is assumed to be constant, resulting in a short unpowered optimal trajectory that is relatively easy to solve. An initial guess was created in the same manner as described in Section III.B.1 for the footprint analysis. However, only the terminal longitude costate was given a nonzero guess as described by Eq. (15). During the continuation process, the terminal mass of the vehicle is reduced to a value that is consistent with the amount of onboard propellant. During this process, the vehicle is able to boost to higher altitudes and faster velocities as shown in Figs. 15 and 16. Note that the altitude axis in Fig. 16 is stretched to highlight the structure of the phugoiding trajectories. The corresponding optimal controls in angle of attack and thrust switch are shown in Fig. 17 where thrust is calculated as shown in Eq. (16). Thrust switch values of positive one indicate the use of maximum thrust, T_{max}, and thrust switch values of negative one indicate the use of no thrust. As expected, the optimal solution consists of an initial boost phase that consumes all available propellant and is followed by a phugoiding coast phase. While optimal phugoiding trajectories have been previously created by direct optimization techniques for high energy aerospace systems,[3,6] this analysis provides confirmation that such trajectories (flown with real aerodynamics and atmosphere models) fully satisfy the necessary conditions of optimality associated with optimal control theory.

$$\lambda_{\theta,f} = -2\theta_f \tag{15}$$

$$T = \frac{T_{\max}}{2}(\text{Thrust Switch} + 1) \tag{16}$$

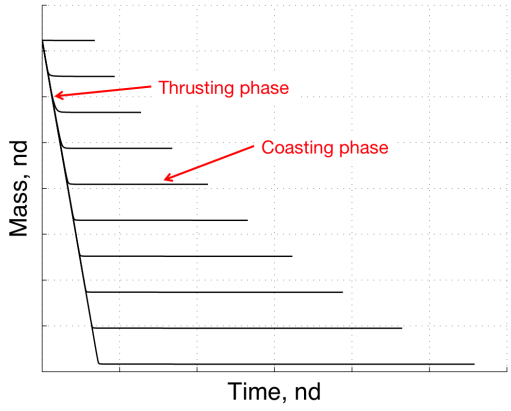

Figure 14: Increased propellant mass during continuation.

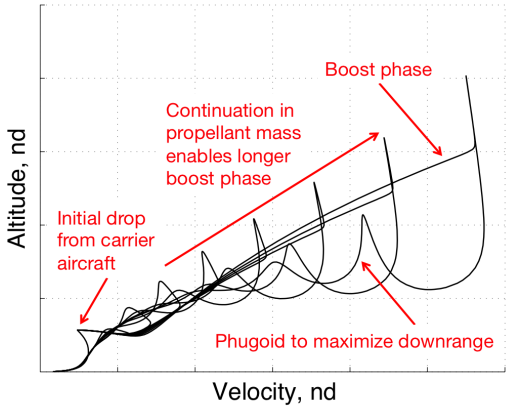

Figure 15: Energy history associated with boost-glide vehicle.

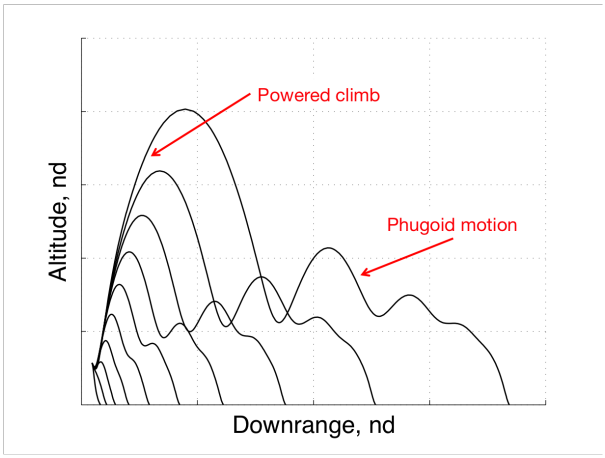

Figure 16: Increased range during continuation.

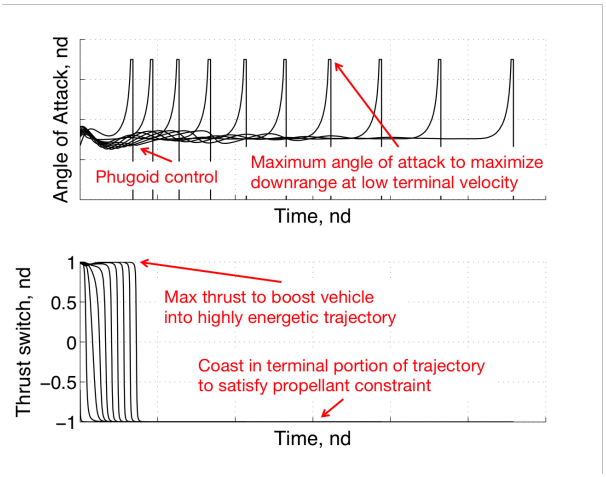

Figure 17: Control history of boost-glide vehicle.

The thrust switch profile (Fig. 17) early in the trajectory highlights the high quality and detailed solutions made possible by the optimal control framework. In the beginning of the thrusting trajectories, a small decrease in thrust is observed. During this phase of flight, the vehicle is falling after release from the carrier aircraft as shown in Figs. 15 and 16. During this phase of flight, it is not efficient to fly at maximum thrust. Instead, it is beneficial to slightly reduce thrust until the vehicle is capable of increasing its flight path angle via angle of attack control (the engines are assumed to have no gimbaling). After the vehicle's descent rate is arrested, maximum thrust is commanded to efficiently boost the vehicle to a high altitude and velocity to maximize downrange. As expected in these minimum terminal energy solutions, the vehicle commands maximum lift during the terminal glide to maximize downrange, resulting in constant terminal flight path angles during the continuation process as shown in Fig. 18.

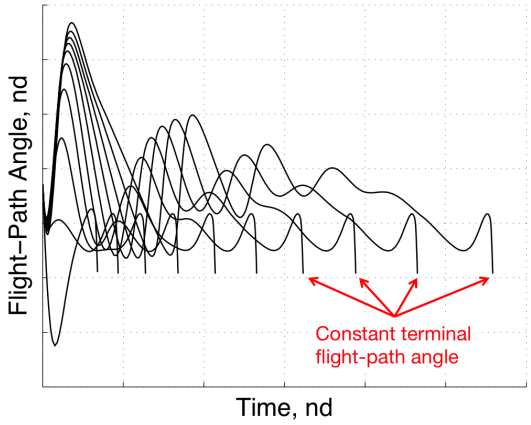

Figure 18: Flight-path angle vs. time.

The corresponding costate histories associated with the continuation process are shown in Fig. 19. The terminal costate values precisely satisfy the necessary conditions of optimality. Since the terminal flight-path angle and velocity are free, the corresponding terminal costates are zero. The terminal longitude costate values are consistent with the necessary condition of optimality associated with the cost functional shown in Eq. (14). In both examples, the continuation procedure proves to be an effective mechanism to construct complex optimal control solutions that include complex costate histories.

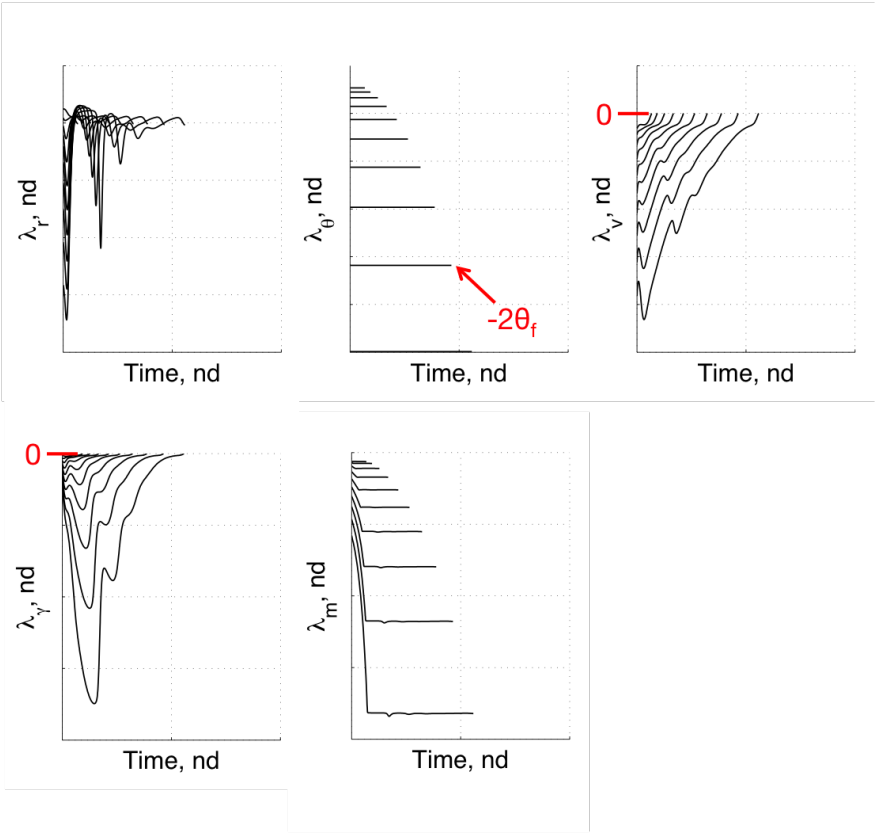

Figure 19: Costate histories associated with boost-glide trajectories.

IV. Conclusions

In this investigation, optimal control solutions are successfully constructed for hypersonic problems that consist of the determination of vehicle performance limitations in downrange and/or crossrange. In these applications, the vehicle travels to a minimum terminal energy state, and modifications to the angle of attack control enable the creation of solutions that fully satisfy the necessary conditions of optimality. These solutions do not require simplification of the equations of motion, predefined control profiles, or significant insight into the optimal solutions. As such, many of the historical limitations associated with optimal control theory can be overcome to address these types of hypersonic problems. The only remaining significant challenge for the designer is the selection of an appropriate continuation policy.

For footprint generation problems, a convenient continuation policy consists of initially fixing the heading of the vehicle into the ultimate direction of crossrange. Starting with a low energy trajectory near the ground, an optimal solution can be easily created that maximizes crossrange by traveling in the direction of the initial heading. After this is completed, the initial state of the vehicle can be changed to increase energy and match the desired set of initial conditions. During this process, the initial heading of the vehicle can be rotated to the desired initial direction. At the end of this process, an optimal crossrange trajectory is created that resides on the footprint. Starting from this optimal solution, the full footprint can be created by performing a continuation of the constrained downrange location. Comparisons with DIDO validate the solutions created by the optimal control framework.

For thrusting applications, a continuation policy of propellant mass enables the construction of long-range, boost-glide trajectories. A smoothing technique for bang-bang solutions enables the numerical solution to common thrusting applications. The high quality solutions generated by the optimal control framework enable the precise calculation of complex control interactions. For thrusting applications, the explicit relationship between thrust and angle of attack as described by the necessary conditions of optimality enable the creation of trajectories with optimal energy management that maximize downrange. The examples presented herein consist of phugoiding trajectories that maximize the distance flown. While the presence of phugoids

in optimal trajectories is not new, this investigation confirms that such trajectories satisfy the necessary conditions of optimality, even when realistic aerodynamic and atmospheric models are used.

Acknowledgements

Approved for Public Release. Distribution Unlimited. Case Number 88ABW-2015-2539.

References

[1]Lu, P. and Xue, S., "Rapid Generation of Accurate Entry Landing Footprints," *Journal of Guidance, Control, and Dynamics*, Vol. 33, No. 3, May 2010, pp. 756–767.

[2]Jorris, T. R. and Cobb, R. G., "Multiple Method 2-D Trajectory Optimization Satisfying Waypoints and No-Fly Zone Constraints," *Journal of Guidance, Control, and Dynamics*, Vol. 31, No. 3, May 2008, pp. 543–553.

[3]Jorris, T. R. and Cobb, R. G., "Three-Dimensional Trajectory Optimization Satisfying Waypoint and No-Fly Zone Constraints," *Journal of Guidance, Control, and Dynamics*, Vol. 32, No. 2, March 2009, pp. 551–572.

[4]Saraf, A., Leavitt, J., Ferch, M., and Mease, K., "Landing Footprint Computation for Entry Vehicles," *AIAA Guidance, Navigation, and Control Conference and Exhibit*, AIAA 2004-4774, Providence, RI, Aug. 2004.

[5]Fahroo, F., Doman, D. B., and Ngo, A. D., "Modeling Issues in Footprint Generation for Reusable Launch Vehicles," *2003 IEEE Aerospace*, IEEE, March 2003, pp. 2791–2799.

[6]Jorris, T., Schulz, C., Friedl, F., and Rao, A., "Constrained Trajectory Optimization Using Pseudospectral Methods," *AIAA Atmospheric Flight Mechanics Conference and Exhibit*, AIAA 2008-6218, Honolulu, HI, Aug. 2008.

[7]Josselyn, S. and Ross, I. M., "Rapid Verification Method for the Trajectory Optimization of Reentry Vehicles," *Journal of Guidance, Control, and Dynamics*, Vol. 26, No. 3, May 2003, pp. 505–508.

[8]Betts, J. T., *Practical Methods for Optimal Control and Estimation Using Nonlinear Programming (Second Edition)*, SIAM, Philadelphia, PA, Nov. 2010.

[9]Grant, M. J. and Braun, R. D., "Rapid Indirect Trajectory Optimization for Conceptual Design of Hypersonic Missions," *Journal of Spacecraft and Rockets*, Vol. 52, No. 1, Jan. 2015, pp. 177–182.

[10]Grant, M., *Rapid Simultaneous Hypersonic Aerodynamic and Trajectory Optimization for Conceptual Design*, Ph.D. thesis, Georgia Institute of Technology.

[11]Silva, C. and Trelat, E., "Smooth Regularization of Bang-Bang Optimal Control Problems," *IEEE Transactions on Automatic Control*, Vol. 55, No. 11, 2010.

[12]Bryson, A. E. and Ho, Y.-C., *Applied Optimal Control*, Taylor and Francis, 1975.